

# A Generic Cycle Life Model for Lithium-ion Batteries Based on Fatigue Theory and Equivalent Cycle Counting

**SOULEMAN N. MOTAPON, (Member, IEEE), ENRIC LACHANCE (Member, IEEE), LOUIS-A. DESSAINT, (FELLOW, IEEE), AND KAMAL AL-HADDAD, (LIFE FELLOW, IEEE)**

Groupe de Recherche en Electronique de Puissance et Commande Industrielle (GREPCI), Ecole de Technologie Supérieure, Université du Québec, Montréal, QC H3C1K3, Canada

Corresponding author: Louis-A. Dessaint (e-mail: louis.dessaint@etsmtl.ca).

**ABSTRACT** This paper proposes a cycle life model for lithium-ion batteries. The main objective of this work is to facilitate the electrical simulation of lithium-ion battery aging (due to cycling), and its impact on battery capacity and internal resistance. Most of the reported cycle life models are either: a) physics based, with parameters difficult to retrieve or b) semi-empirical, where the parameter identification process requires large amount of experimental data, huge manpower and test duration lasting from months to years. Moreover, these models tend to be valid only for the underlying battery and not for other battery types. This makes the simulation of lithium-ion batteries cycling effects, difficult to achieve, expensive and time consuming. The model proposed in this paper is based on simple physical equations from fatigue theory and equivalent cycle counting. The parameter identification process is straightforward and requires only few data from battery datasheets and limited (or short duration) cycling experiments. The proposed model is generic and able to represent the impact of common cycle life factors such as: depth-of-discharge (DoD), temperature and C-rate. The model is validated using two lithium-ion battery types (LFP-LiFePO<sub>4</sub> and NMC-LiNiMnCoO<sub>2</sub>) and simulation results are close to reality with an error within  $\pm 1.5\%$  compared to experimental results.

**INDEX TERMS** Battery cycle life model, capacity loss curves, equivalent cycle counting, generic battery model, lithium-ion batteries.

## I. INTRODUCTION

Lithium-ion batteries are the energy storage of choice in many applications including transportation (cars, buses, trains, aircraft, etc.), portable electronics and back-up power systems. This is mainly due to their high energy and power densities, high efficiency as well as low self-discharge compared to their counterparts (NiCd, NiMH and Lead Acid) [1]–[6].

Like other battery types, the energy and power densities of lithium-ion batteries diminish with aging. This is due to change in battery capacity and internal resistance as the battery ages [7]–[12]. This aging effect is amplified when the battery operates, principally due to cycling at different operating conditions. In order to properly estimate the battery state-of-charge (SoC) while the battery is in operation, and ensure the load demand (over the battery lifetime) is fulfilled, a cycle life model is required.

Several cycle life models of lithium-ion batteries have been reported in the literature. They are either electrochemical/physics based or empirical/semi-empirical based.

The electrochemical or physics-based models use complex

differential equations with lots of in-depth parameters (such as electrode volume, separator thickness, ion concentration, reaction rate, etc.) [13], [14]. These models are able to represent the physical changes in electrode and electrolyte (e.g. growth of the solid electrolyte interphase (SEI) layer, loss of ions and active material, growth of deposit layer, loss of electrolyte, etc.) due to cycling and their impact on the battery cell performance. However, these models are not realistic for electrical simulation as the model parameters are not easily available and difficult to retrieve.

The empirical or semi-empirical models are based on large amount of experimental data and semi-empirical equations or look-up tables [15]–[24]. The Ah-throughput (or coulomb counting) modeling approach proposed in [15]–[19] is the most popular example of this category. In these models, the capacity loss and resistance growth due to cycling are estimated using empirical equations of several unknown parameters. The identification of parameters usually requires cycling experiments lasting years in a controlled testing environment. This makes these models expensive to characterize and time consuming. Moreover, as demonstrated in [25] and [26],



these models tend to be valid only for the specific battery under test and not applicable for a different battery type.

Some authors have also proposed cycle life models where the battery cycle number is computed using the rain flow counting (RFC) algorithm, widely used in fatigue analysis [27], [28]. These models can only be used off-line as it requires a *priori* knowledge of the loading profile. Hence the impact of cycling on the battery capacity and internal resistance can not be represented while the battery is in operation.

In this paper, a cycle life model based on physical equations from fatigue theory and equivalent cycle counting is proposed. For every charge-discharge cycle, an aging index is computed based on the equivalent cycle number and stress factors associated to DoD, C-rate, and temperature. This aging index is then used to represent the impact of cycling on the battery capacity and internal resistance. The model parameters are derived using life cycle (or capacity loss) curves provided on battery datasheet and limited (or short duration) cycling experiments. The model is generic and can be used for any lithium-ion battery types.

Key contributions of this paper are:

- a cycle life model with a simplified and quick approach for parameter identification using battery datasheet and limited (or short duration) cycling experiments. As most lithium-ion battery datasheets come with life cycle curves, the parameter identification process is less time consuming.
- the model is based on physical equations and equivalent cycle counting, which makes it applicable to any type of lithium-ion battery.
- this work is an improvement to previous work reported in [29], in which a cycle life model is added to represent cycling effects on the battery model performance.

The next section describes the proposed cycle life model, the third section shows the procedure to extract model parameters from datasheets and experiments, and finally, the fourth section deals with the experimental validation.

## II. THE CYCLE LIFE MODEL

Fig. 1 shows an improved version of the battery model from [29], which includes the proposed cycle life model. The battery model is represented by Block A, as a variable open circuit voltage ( $E$ ) in series with a resistance. The open circuit voltage and resistance depend on the battery thermodynamics voltage ( $E_0$ ), battery capacity ( $Q$ ), internal resistance ( $R$ ) and polarization constant ( $K$ ). As  $E_0$ ,  $Q$ ,  $R$  and  $K$  vary with battery temperature, a thermal model (Block B-D) is added in [29] to estimate these parameters. Block C estimates the heat generated by the battery and Block B estimates the battery temperature. Block D calculates  $E_0$ ,  $Q$ ,  $R$  and  $K$  using the estimated battery temperature. The cycle life model (Block E) is used to modify the battery capacity and resistance based on battery age. This paper focuses only on the cycle life block (Block E). Details on the other blocks (A-D) are fully covered in [29].

The cycle life model consists of four main blocks (Block E1-E4). Block E1 determines the depth-of-discharge (DoD) and average C-rate during each cycle. Block E2 estimates the maximum number of cycles based on stress factors associated to ambient temperature, DoD, and C-rate. The aging index is computed in Block E3 based on the concept of equivalent number of cycles. Finally, Block E4 adjusts the battery capacity and resistance based on the aging index. The following sections present modeling equations for each block.

### A. DOD AND AVERAGE C-RATE CALCULATION (BLOCK E1)

Figs. 2–3 show Block E1 outputs (DoD and C-rates), for a typical SoC and battery current profiles.

The DoD during each cycle is computed when the battery transition from charge to discharge or discharge to charge. This is accomplished by looking at the change of SoC ( $\Delta\text{SoC}$ ) over a small-time step  $\Delta T$ . A transition is detected when the sign of  $\Delta\text{SoC}$  differs from the one calculated in the previous time step.

Equation (1) is used to calculate the change of SoC at every time step  $\Delta T$ .

$$\Delta\text{SoC}(k) = \text{SoC}(k) - \text{SoC}(k-1) \quad (1)$$

where  $\text{SoC}(k)$  is the sampled SoC at time  $k \cdot \Delta T$  ( $k = 1, 2, 3, \dots, \infty$ ).

The DoD is calculated using the following algorithm:

Step 1: Initialize the number of transitions,  $n_{\text{prev}} = 1$ , and DoD,  $\text{DoD}(1) = 1 - \text{SoC}_{\text{init}}$ , where  $\text{SoC}_{\text{init}}$  is the battery initial SoC.

Step 2: At every time step  $\Delta T$ , evaluate  $\Delta\text{SoC}(k)$ . If sign  $\Delta\text{SoC}(k) \neq \text{sign } \Delta\text{SoC}(k-1)$ ,

- Increment number of transitions,  $n = n_{\text{prev}} + 1$ .
- Calculate DoD as follows,

$$\text{DoD}(n) = 1 - \text{SoC}(k) \quad (2)$$

- Store number of transitions,  $n_{\text{prev}} = n$ .

The average C-rates,  $I_{\text{dis\_ave}}$  and  $I_{\text{ch\_ave}}$  during discharge and charge respectively, are also evaluated at discharge-charge or charge-discharge transition using the following algorithm:

Step 1: Initialize the number of samples,  $a_{\text{prev}} = 0$ , the number of transitions,  $n_{\text{prev}} = 1$ , and C-rates,  $I_{\text{dis\_ave}}(1) = I_{\text{Batt\_init}}$ ,  $I_{\text{ch\_ave}}(1) = I_{\text{Batt\_init}}$ , where  $I_{\text{Batt\_init}}$  is the battery initial current.

Step 2: At every time step  $\Delta T$ , evaluate  $\Delta\text{SoC}(k)$ . If sign  $\Delta\text{SoC}(k) \neq \text{sign } \Delta\text{SoC}(k-1)$ ,

- Increment number of transitions,  $n = n_{\text{prev}} + 1$ .
- Calculate number of samples,  $a = k$ .
- Calculate  $I_{\text{dis\_ave}}$  and  $I_{\text{ch\_ave}}$  as follows,
  - if  $\Delta\text{SoC}(k) > 0$

$$I_{\text{dis\_ave}}(n) = \frac{1}{M} \sum_{k=a_{\text{prev}}}^{a-1} |I_{\text{Batt}}(k)| \quad (3)$$

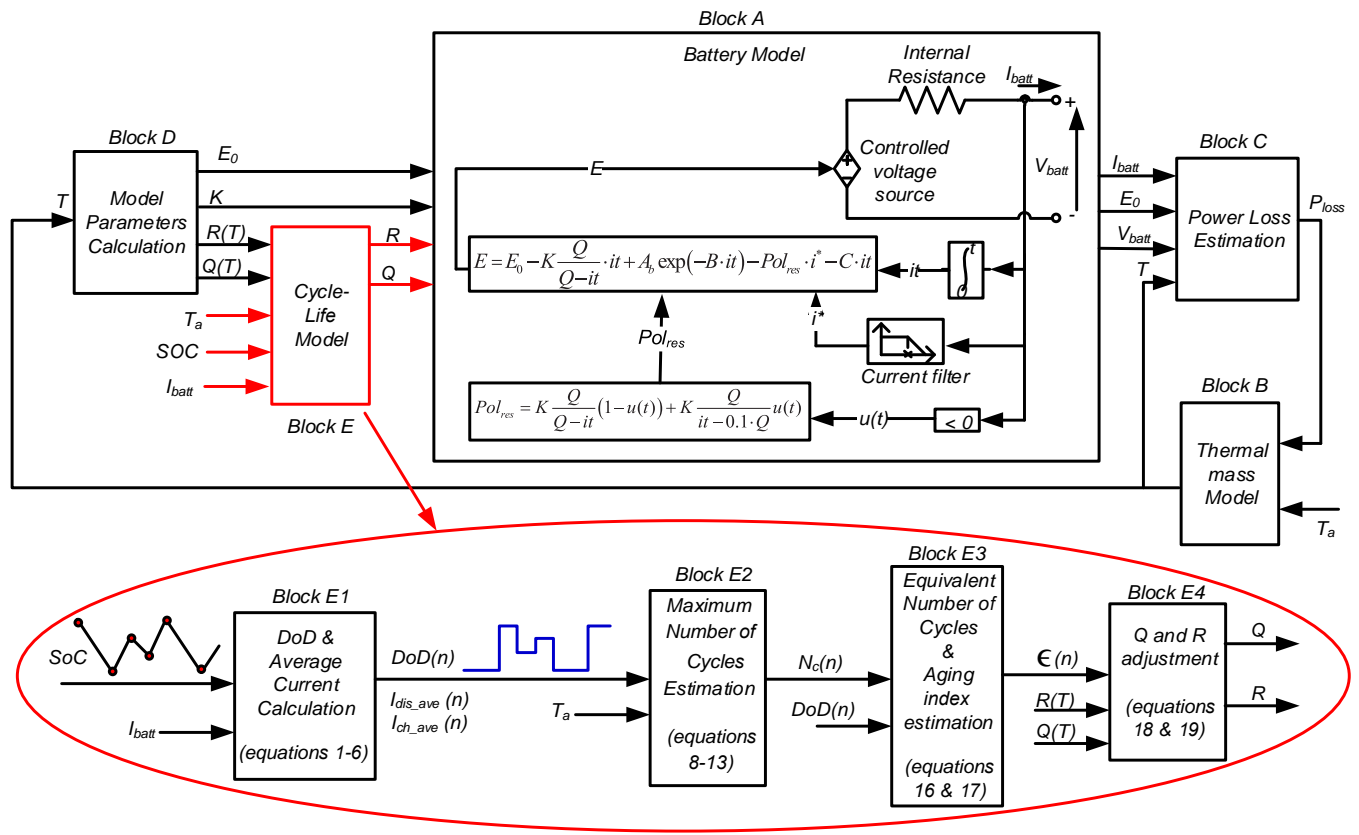


**FIGURE 1.** Proposed lithium-ion battery cycle life model.

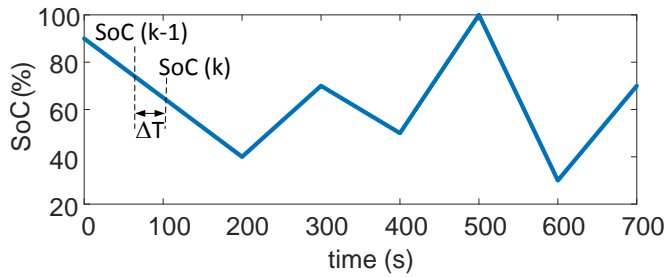


**FIGURE 2.** DoD estimation during each cycle.

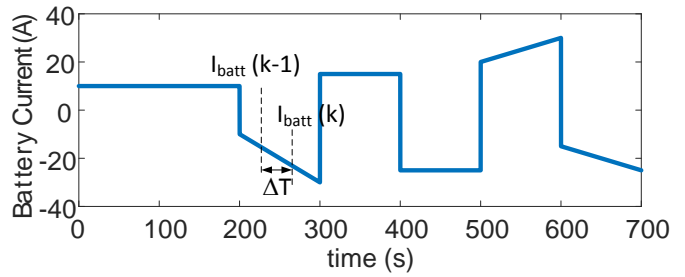


**FIGURE 3.** C-rate estimation during each cycle.

and,

$$I_{ch\_ave}(n) = I_{ch\_ave}(n-1) \quad (4)$$

- if  $\Delta SoC(k) \leq 0$

$$I_{dis\_ave}(n) = I_{dis\_ave}(n-1) \quad (5)$$

and,

$$I_{ch\_ave}(n) = \frac{1}{M} \sum_{k=a_{prev}}^{a-1} |I_{Batt}(k)| \quad (6)$$

where  $M = a - a_{prev}$  is the number of samples between two transitions.



- Store the number of samples,  $a_{prev} = a$ , and the number of transitions,  $n_{prev} = n$ .

### B. MAXIMUM NUMBER OF CYCLE ESTIMATION (BLOCK E2)

The maximum number of cycles is defined as the battery number of cycles to end-of-life (EoL), when subjected to a repetitive discharge and charge cycle at a given DoD, C-rates, and temperature. A battery is considered to have reached its EoL when it has lost 20% of its initial capacity. The maximum number of cycles is evaluated from the resulting stress factor (or stress per cycle), caused by the DoD, C-rates, and temperature.

As shown in [30]–[33] the battery aging due to cycling is analogous to material degradation due to cumulative cyclic stress, and equations from fatigue analysis are applicable for battery cycle-life studies. In [33], the degradation ( $D$ ) per cycle is calculated using Wöhler approximation and Miner's rule as:

$$\frac{D}{Cycle} = \left( \frac{\sigma_{amp}}{\sigma_{Yield}} \right)^{\frac{1}{m}} \quad (7)$$

where,  $\sigma_{amp}$  is the stress amplitude that the material is subjected to,  $\sigma_{Yield}$  is the peak stress that the material can sustain (or its yield strength) and  $m$  is the fatigue strength exponent.

By analogy, if the stress per cycle, due to the DoD, has an amplitude,  $DoD(n)$ , with a peak stress amplitude,  $DoD_{ref} = 100\%$ , then the stress factor ( $\theta_{DoD}$ ) associated to DoD can be computed as:

$$\theta_{DoD}(n) = \left( \frac{DoD(n)}{DoD_{ref}} \right)^{\frac{1}{\xi}} \quad (8)$$

where,  $\xi$  is the stress exponent for the DoD.

Similarly, the stress factor due to C-rates are computed as:

$$\theta_{I\_dis}(n) = \left( \frac{I_{dis\_ave}(n)}{I_{dis\_ref}} \right)^{\frac{1}{\gamma_1}} \quad (9)$$

And,

$$\theta_{I\_ch}(n) = \left( \frac{I_{ch\_ave}(n)}{I_{ch\_ref}} \right)^{\frac{1}{\gamma_2}} \quad (10)$$

where  $\theta_{I\_dis}(n)$  and  $\theta_{I\_ch}(n)$  are the stress factors associated to the discharge and charge current, respectively.  $I_{dis\_ref}$  and  $I_{ch\_ref}$  are the peak stress amplitudes for the discharge and charge current, respectively.  $\gamma_1$  and  $\gamma_2$  are the stress exponents for the discharge and charge current, respectively. The stress factor ( $\theta_T$ ) due to temperature is computed using the Arrhenius equation as [32]:

$$\theta_T(n) = \exp \left[ -\psi \left( \frac{1}{T_a(n)} - \frac{1}{T_{ref}} \right) \right] \quad (11)$$

where  $T_a(n)$  and  $T_{ref}$  are the ambient and reference temperatures, respectively, during each cycle.  $\psi$  is the Arrhenius rate constant.

The resulting or combined stress factor ( $\theta$ ) is computed as [32]:

$$\theta(n) = \theta_{DoD}(n) \prod \theta_{I\_dis}(n) \prod \theta_{I\_ch}(n) \prod \theta_T(n) \quad (12)$$

The maximum number of cycles ( $N_c$ ) to EoL is inversely proportional to the resulting stress factor and is computed as [33]:

$$\begin{aligned} N_c(n) &= \frac{N_{c\_ref}}{\theta(n)} \\ &= N_{c\_ref} \left( \frac{DoD(n)}{DoD_{ref}} \right)^{-\frac{1}{\xi}} \\ &\cdot \left( \frac{I_{dis\_ave}(n)}{I_{dis\_ref}} \right)^{\frac{-1}{\gamma_1}} \cdot \left( \frac{I_{ch\_ave}(n)}{I_{ch\_ref}} \right)^{\frac{-1}{\gamma_2}} \\ &\cdot \exp \left[ -\psi \left( \frac{1}{T_{ref}} - \frac{1}{T_a(n)} \right) \right] \end{aligned} \quad (13)$$

where  $N_{c\_ref}$  is the maximum number of cycles when the battery is subjected to a repetitive discharge and charge cycle at DoD =  $DoD_{ref}$ , C-rates =  $(I_{dis\_ref}, I_{ch\_ref})$  and temperature =  $T_{ref}$ .

### C. AGING INDEX ESTIMATION (BLOCK E3)

The aging index represents the contribution of applied cycles to the total aging of the battery. If the battery is subjected to a repetitive discharge and charge cycle at DoD =  $DoD_{ref}$ , C-rates =  $(I_{dis\_ref}, I_{ch\_ref})$  and ambient temperature =  $T_{ref}$  (i.e. the battery is discharged from 100% SoC to 0% SoC, and then recharged to 100% SoC), the aging index after one cycle is given by:

$$\epsilon = \frac{1}{N_{c\_ref}} \quad (14)$$

Knowing that for realistic load profiles, a discharge (or charge) cycle may not always start (or end) with battery SoC of 100%, the concept of equivalent number of cycles is introduced. The equivalent number of cycles for a given DoD is defined as the number of cycles equivalent to the scenario where the SoC at the beginning and end of cycle is 100%. For example, if the battery is discharged from 80% SoC (20% DoD) to 40% SoC (60% DoD), and then recharged to 60% SoC (40% DoD). The cycle's DoD is 60% and the equivalent number of cycles is given by (see Fig. 4):

$$N_{eq} = 0.5 \left( 1 - \frac{20\%}{60\%} \right) + 0.5 \left( 1 - \frac{40\%}{60\%} \right) \quad (15)$$

As (13) only applies to cycles starting and ending with 100% SoC, the concept of equivalent number of cycles allows computation of aging index when the battery is subjected to any given DoD swing.

By applying (15) to Fig. 2, the equivalent number of cycles after each cycle is computed as:

$$N_{eq}(n) = 0.5 \left( 2 - \frac{DoD(n-2) + DoD(n)}{DoD(n-1)} \right) \quad (16)$$

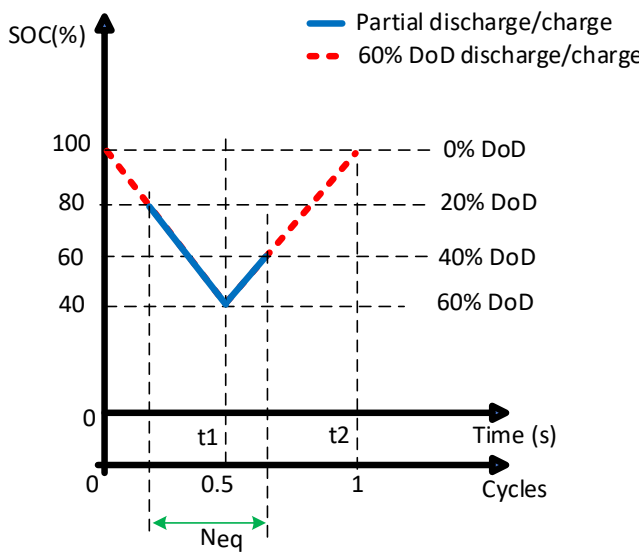


**FIGURE 4.** Equivalent number of cycle concept.

The aging index after each cycle is given as:

$$\epsilon(n) = \epsilon(n-1) + \frac{N_{eq}(n)}{N_c(n-1)} \quad (17)$$

#### D. BATTERY CAPACITY AND RESISTANCE ESTIMATION (BLOCK E4)

The battery capacity and resistance are determined based on the aging index. As discussed in [34], the battery capacity and resistance exhibit a nonlinear characteristic with aging. This is mainly due to nonlinear growth of the SEI (solid electrolyte interphase) layer and nonlinear loss of lithium-ions, active material, and electrolyte as the battery ages.

The battery capacity ( $Q$ ) and resistance ( $R$ ) are expressed (considering the nonlinear effect of aging) as follows:

$$Q(n) = Q_{BoL} - \epsilon(n)^\alpha \cdot (Q_{BoL} - Q_{EoL}) \quad (18)$$

$$R(n) = R_{BoL} + \epsilon(n)^\beta \cdot (R_{EoL} - R_{BoL}) \quad (19)$$

where,  $Q_{BoL}$  and  $Q_{EoL}$  are the battery capacity (Ah) at BoL (beginning of life) and EoL, respectively.  $R_{BoL}$  and  $R_{EoL}$  are the battery resistance ( $\Omega$ ) at BoL and EoL, respectively.  $\alpha$  and  $\beta$  are the aging exponents for the battery capacity and resistance, respectively.  $Q_{EoL}$  is assumed to be 80% of  $Q_{BoL}$ .  $Q_{BoL}$  and  $R_{BoL}$  correspond to  $Q(T)$  and  $R(T)$  of Block D (see Fig. 1), respectively.

#### III. IDENTIFICATION OF MODEL PARAMETERS

Equation (13) requires identification of five parameters ( $N_{c\_ref}$ ,  $\xi$ ,  $\gamma_1$ ,  $\gamma_2$ ,  $\psi$ ). These parameters are determined using life cycle curves (capacity loss vs. cycles) at different cycling conditions.

Battery datasheets along with limited (or short duration) cycling experiments are used to identify the model parameters. The experiments consist of cycling four batteries simultaneously, and at different conditions, until their capacity is

reduced by 5%. For each cycling conditions, only one cycle life factor (DoD, C-rates or temperature) is varied in order to detect their individual effects. The 5% number is selected in order to get a significant impact of each cycle life factor on the battery aging process.

The aging exponents ( $\alpha$  and  $\beta$ ) are also determined from capacity loss and resistance growth curves at nominal cycling conditions. As the resistance growth curve (resistance vs. cycles) is seldom provided on datasheet, the battery resistance is measured experimentally, every few number of cycles.

Fig. 5 shows typical data points required from datasheets or experiments. As shown (see curve in blue), at least one full life cycle curve (i.e. battery cycling until EoL) is required. As this data can be retrieved in most datasheets, a full life cycle test is not necessary. This makes the duration of cycling experiments less time consuming.

The aging exponent,  $\alpha$ , is estimated using (18), at nominal cycling condition ( $T_a = T_1$  °C, DoD = 100%, I-discharge =  $I_{d1}$ , I-charge =  $I_{c1}$ ), as follows:

$$\alpha = \frac{\ln\left(\frac{Q_{BoL}-Q_5}{Q_{BoL}-Q_{EoL}}\right)}{\ln\left(\frac{N_2}{N_{c2}}\right)} \quad (20)$$

Similarly,  $\beta$  is given (using (19)) as:

$$\beta = \frac{\ln\left(\frac{R_5-R_{BoL}}{R_{EoL}-R_{BoL}}\right)}{\ln\left(\frac{N_2}{N_{c2}}\right)} \quad (21)$$

where  $Q_5$  is 95% of  $Q_{BoL}$ .  $N_2$  and  $N_{c2}$  are the number of cycles when the capacity are  $Q_5$  and  $Q_{EoL}$ , respectively.  $R_5$  is the battery resistance when the capacity is  $Q_5$ .

The numbers of cycles to EoL ( $N_{c1}$ ,  $N_{c3}$ ,  $N_{c4}$ ,  $N_{c5}$ ) for other cycling conditions are estimated using (18) as:

$$N_{cj} = \frac{N_{c2} \cdot N_j}{N_2} \quad (22)$$

where  $j \in (1, 3, 4, 5)$ .  $N_j$  is the number of cycles when the capacity is  $Q_5$ , for each cycling condition as shown in Fig. 5.

The model parameters ( $N_{c\_ref}$ ,  $\xi$ ,  $\gamma_1$ ,  $\gamma_2$ ,  $\psi$ ) are estimated using (13) as follows:

$$N_{c\_ref} = N_{c2} \quad (23)$$

$$\xi = -\frac{\ln(0.25)}{\ln\left(\frac{N_{c1}}{N_{c2}}\right)} \quad (24)$$

$$\gamma_1 = -\frac{\ln\left(\frac{I_{d2}}{I_{d1}}\right)}{\ln\left(\frac{N_{c4}}{N_{c2}}\right)} \quad (25)$$

$$\gamma_2 = -\frac{\ln\left(\frac{I_{c2}}{I_{c1}}\right)}{\ln\left(\frac{N_{c3}}{N_{c2}}\right)} \quad (26)$$

$$\psi = \frac{\ln\left(\frac{N_{c5}}{N_{c2}}\right)}{\frac{1}{T_2} - \frac{1}{T_1}} \quad (27)$$

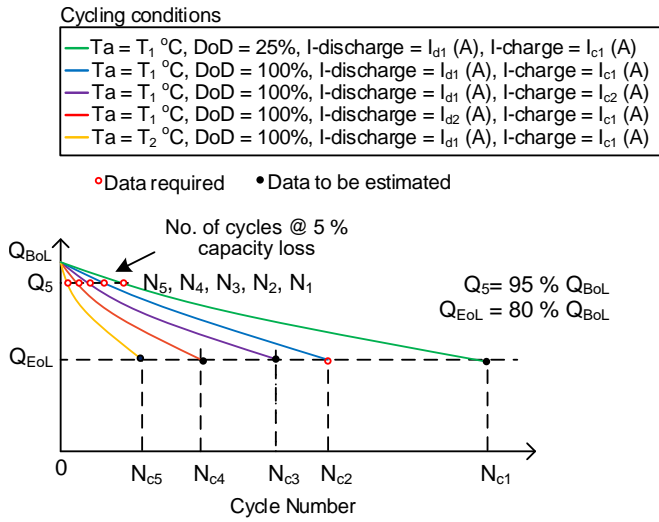


**FIGURE 5.** Typical data points required for model parameters identification. Red dots indicates extracted data points and black dots are estimated data.

#### IV. EXPERIMENTAL VALIDATION

The proposed cycle life model is validated using two lithium-ion battery chemistry (LFP-LiFePO<sub>4</sub> and NMC-LiNiMnCoO<sub>2</sub>). For validation purposes, a test bench which includes a thermal test chamber is used to perform accelerated cycling tests at different cycling conditions. As shown in Fig. 5, at least four life cycle curves are required for model parameters identification (number of tests can be reduced based on data available from battery datasheets). The following section briefly describes the test bench setup (shown in Fig. 6).

##### A. TEST BENCH SETUP

The test bench setup consists of the following:

- an environmental test chamber (Thermotron XSE-600).
- a battery analyser/cycler (PCBA 5010-4) with 4 channels, to cycle up to 4 battery cells simultaneously.
- 5 LiFePO<sub>4</sub> battery cells, 3.3 V, 2.5 Ah, 26650 cylindrical from A123 system.
- 5 LiNiMnCoO<sub>2</sub> battery cells, 3.7 V, 2000 mAh, 18650 cylindrical generic batteries.

For the LiFePO<sub>4</sub> battery, model parameters are identified using life cycle curves from datasheet and experimental tests. The cycling conditions are summarized in Table 1.

As shown in Table 1, three experimental tests at room temperature are required for the LiFePO<sub>4</sub> battery. Each cycling test starts with a capacity and resistance tests to determine the BoL capacity and resistance. At every  $\Delta n$  number of cycles ( $\Delta n$  is equal to 5 cycles near the BoL and EoL, and 50 cycles in between), the cycling is interrupted and a capacity and resistance tests are initiated to determine the current capacity and resistance. The test sequence continues until the capacity reaches 95% of its initial value. During cycling of fresh LFP battery cells, the capacity was increasing before dropping to its nominal value during the first few cycles (50 to 100

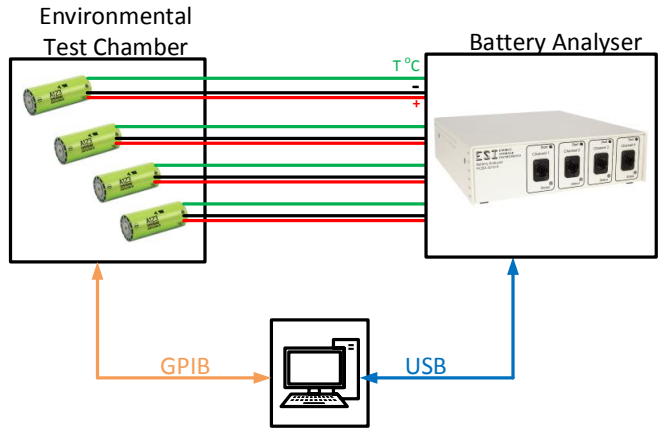


**FIGURE 6.** Test bench setup.

Cell #	1	2	3	4*	5*
<b>DoD</b>	100 %	100 %	25 %	100 %	100 %
<b>Discharge rate</b>	2 C	2 C	2 C	8 C	2 C
<b>Charge rate</b>	1 C	1.5 C	1.5 C	1.2 C	1.2 C
<b>Temperature</b>	23°C	23°C	23°C	23°C	45°C

\* Datasheet Curves

**TABLE 1.** Cycling conditions for parameters identification, LiFePO<sub>4</sub> battery.

cycles). For the NMC, this phenomenon was less noticeable. Data recording was initiated as soon as this phenomenon was completed, i.e. when the battery started to age.

Figs. 7–10 show the simulation and experimental results at cycling conditions of Table 1. As shown, the impact of each life cycle factor on the LiFePO<sub>4</sub> battery, is well represented by the proposed model, with an absolute error of less than 1%.

Table 2 shows data extracted from datasheet and experiments along with model parameters, for the LFP battery type. Fig. 11 shows the estimated stress factors per cycle due to DoD, C-rates and ambient temperature.

For validation purpose, two additional cycling tests were performed at operating conditions that differ from those used for parameters identification. Fig. 12 shows the simulation and experimental results when the LFP battery is cycled at 100% DoD, with C-rates of 1C(charge)/3C(discharge) at 21 °C and 43 °C ambient temperatures. As shown, the results

Input data for parameters identification					
$N_1$	$N_2$	$N_3$	$N_4$	$N_5$	$N_{c2}$
10312	2200	1850	390	930	9175
Model parameters (estimated)					
$N_{c\_ref}$	$\xi$	$\psi$	$\gamma_1$	$\gamma_2$	$\alpha$
9175	0.8	3.7e3	0.8	2.34	0.9708

**TABLE 2.** Model parameters for the LFP battery.

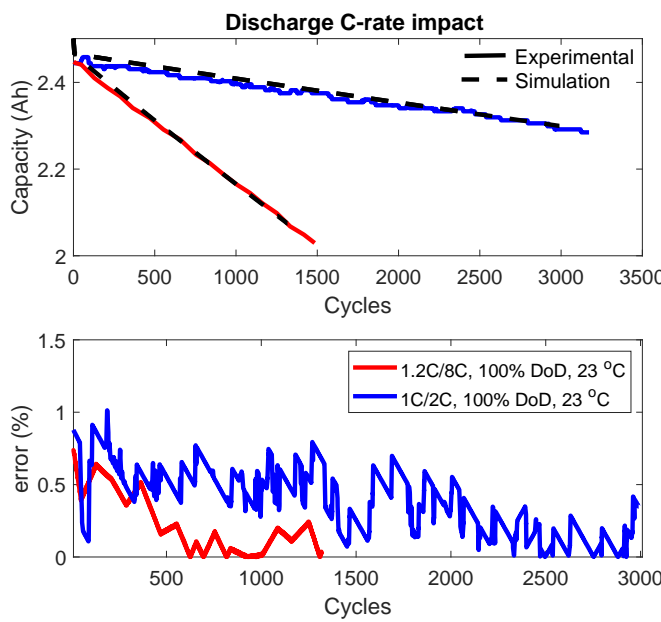


FIGURE 7. Impact of discharge C-rate on the LFP battery life cycle.

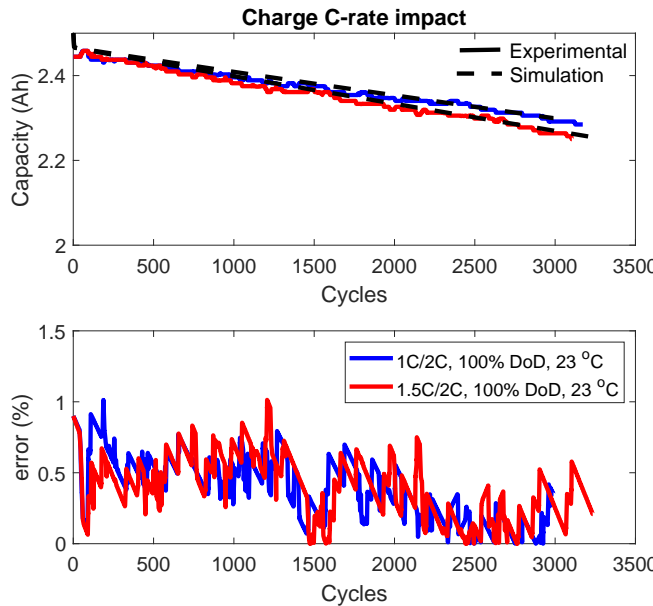


FIGURE 8. Impact of charge C-rate on the LFP battery life cycle.

are close to reality with a maximum absolute error of 1% and 1.5 % at 21 °C and 43 °C, respectively.

For the NMC battery, the model parameters were extracted from five cycling tests as shown in Table 3. Tests were conducted in the same manner as for the LFP battery.

Figs. 13–16 show the simulation and experimental results at cycling conditions of Table 3. As shown, the impact of each life cycle factor on the LiNiMnCoO<sub>2</sub> battery, is also well represented by the proposed model, with an absolute error of less than 1.5%.

Table 4 summarizes the models parameters for the NMC battery.

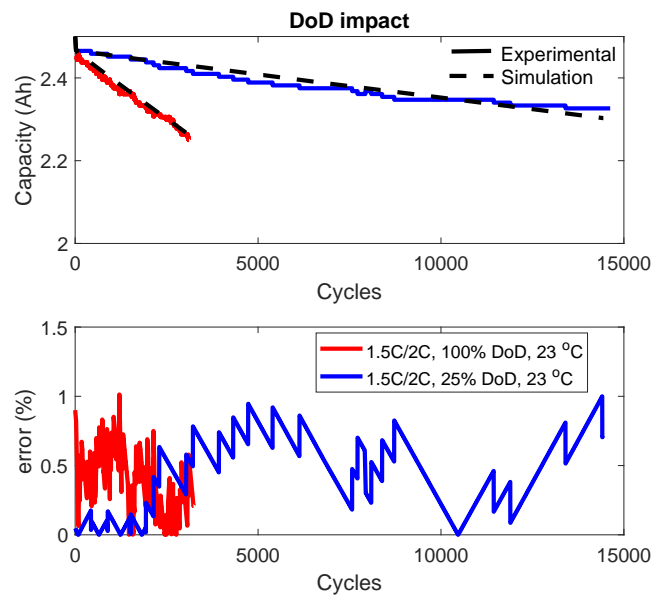


FIGURE 9. Impact of DoD on the LFP battery life cycle.

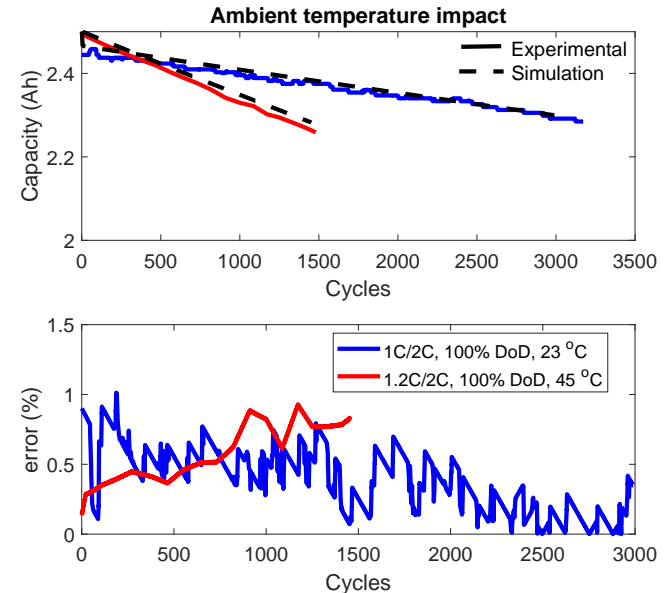
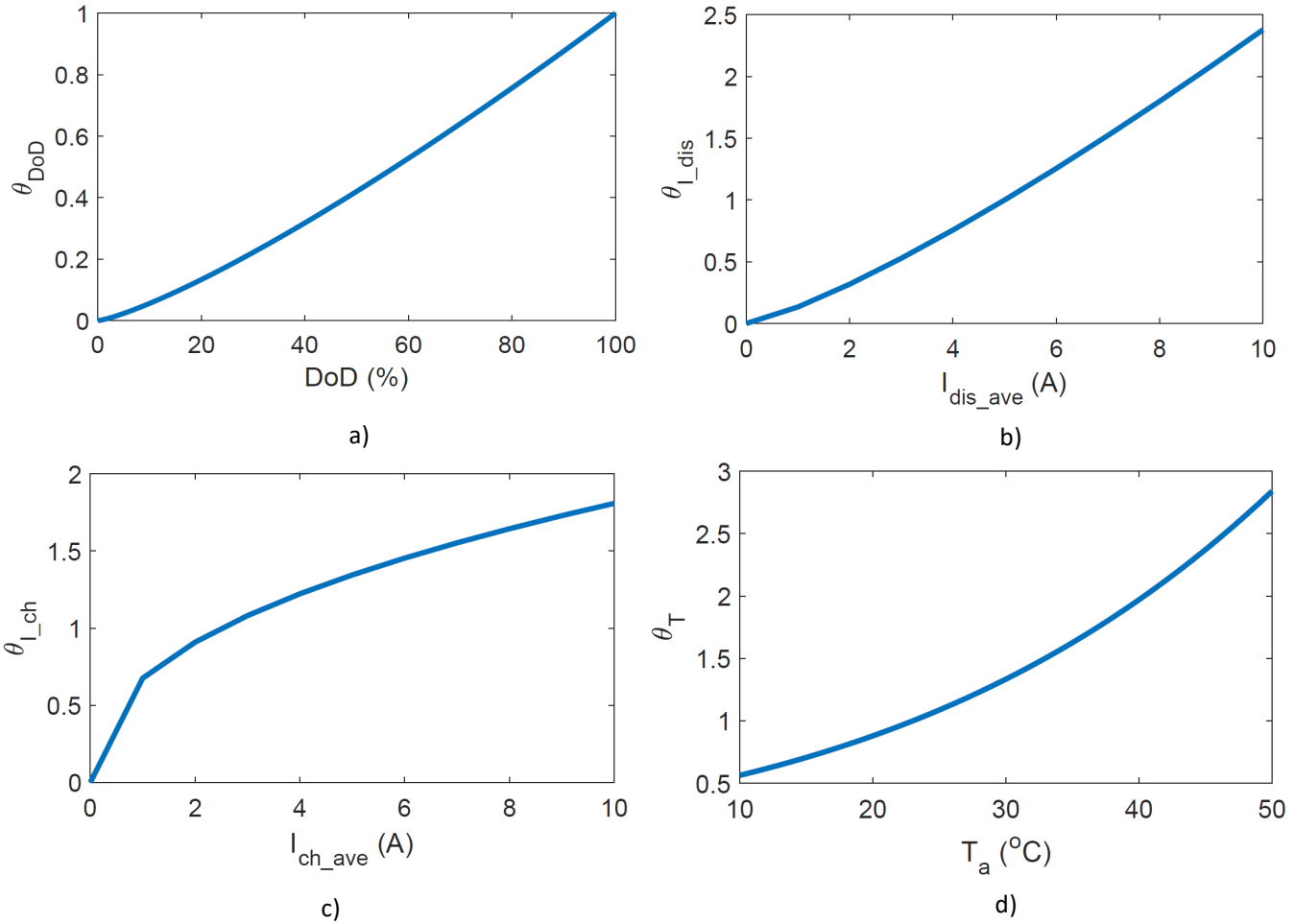


FIGURE 10. Impact of ambient temperature on the LFP battery life cycle.

Cell #	1	2	3	4	5
DoD	100 %	100 %	100 %	25 %	100 %
Discharge rate	0.8 C	0.8 C	1.5 C	0.8 C	0.8 C
Charge rate	0.8 C	1.5 C	0.8 C	0.8 C	0.8 C
Temperature	25°C	25°C	25°C	25°C	45°C

TABLE 3. Cycling conditions for parameters identification, LiNiMnCoO<sub>2</sub> battery.



**FIGURE 11.** Estimated stress factors per cycle due to: a) DoD, b) discharge C-rate, c) charge C-rate and d) ambient temperature.

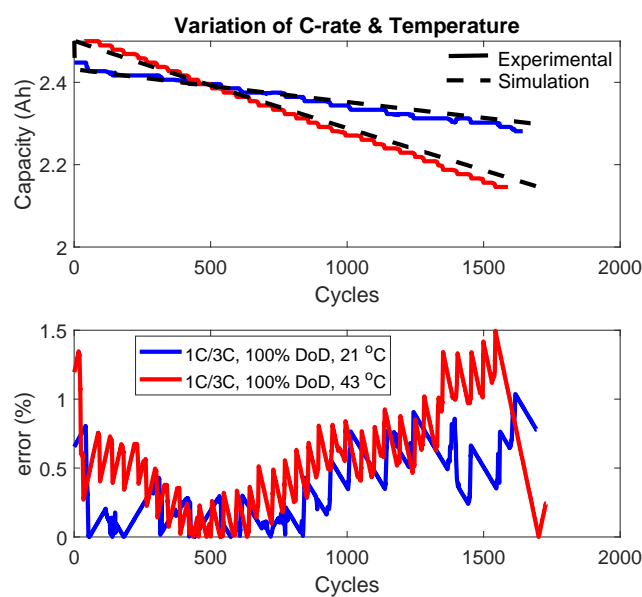


**FIGURE 12.** Model performance at different cycling conditions.

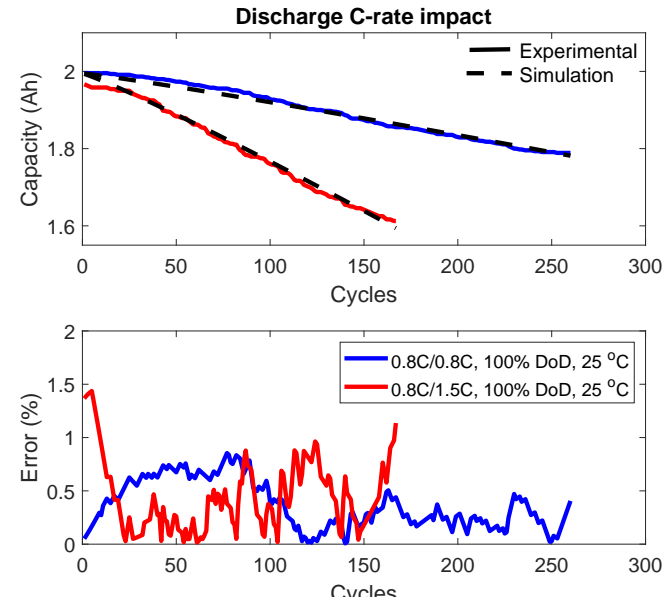


**FIGURE 13.** Impact of discharge C-rate on the NMC battery life cycle.

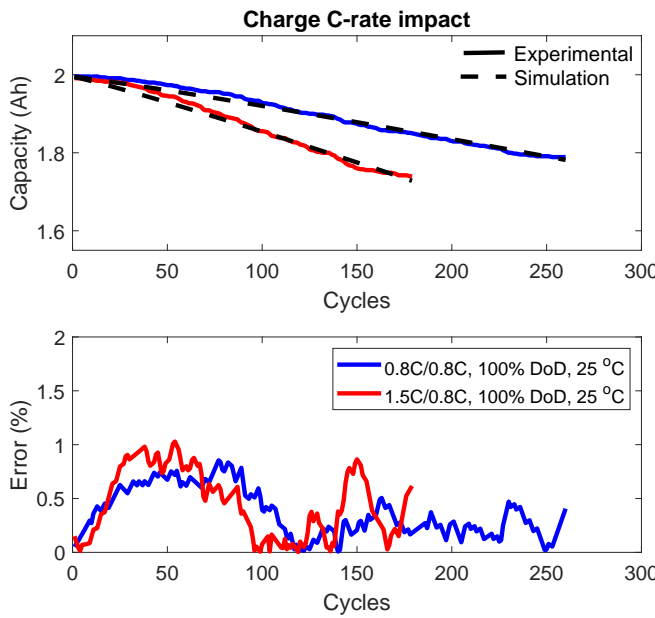


FIGURE 14. Impact of charge C-rate on the NMC battery life cycle.

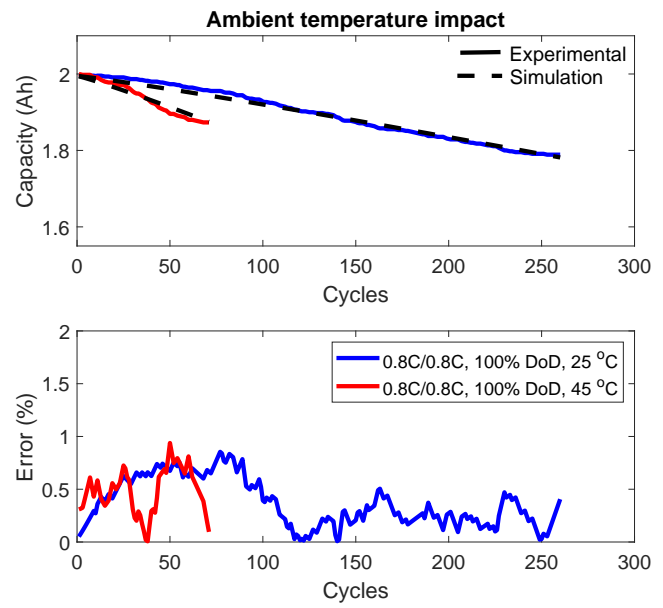


FIGURE 16. Impact of ambient temperature on the NMC battery life cycle.

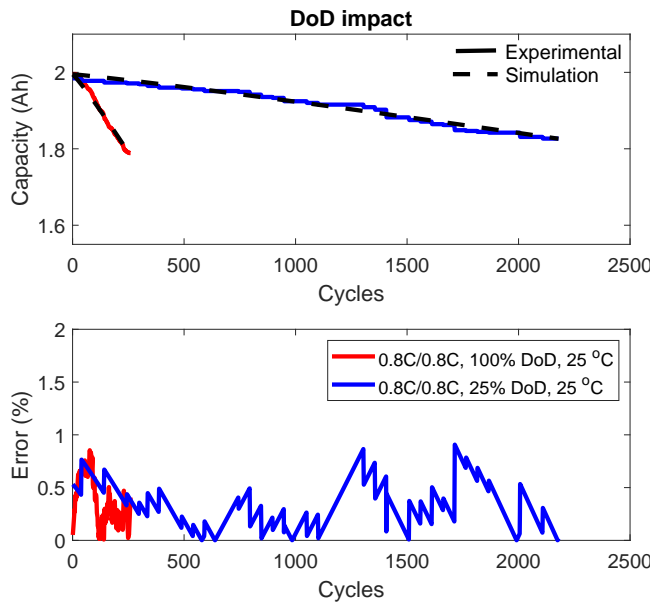


FIGURE 15. Impact of DoD on the NMC battery life cycle.

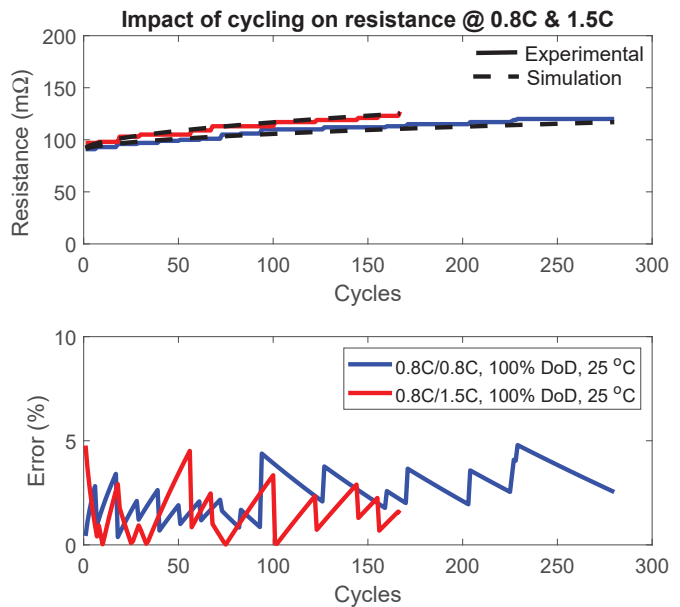


FIGURE 17. Impact of cycling at 0.8C and 1.5C discharge C-rates on battery resistance.

It was noted from experiments that the battery resistance did not change much for the LFP battery, whereas for the NMC, there was a 39 % increase at the EoL. The resistance growth results for the NMC battery are shown in Figs. 17-18. The aging exponent,  $\beta = 0.5262$  (computed using (21) with  $R_5=108 \text{ m}\Omega$ ,  $R_{BoL}=90 \text{ m}\Omega$  and  $R_{EoL}=125 \text{ m}\Omega$ ).

As shown from Figs. 17-18, the proposed model is able to represent the impact of cycling on battery resistance with less than 5% absolute error.

Input data for parameters identification					
$N_1$	$N_2$	$N_3$	$N_4$	$N_5$	$N_{c2}$
1350	130	73	47	60	460
Model parameters (estimated)					
$N_{c\_ref}$	$\xi$	$\psi$	$\gamma_1$	$\gamma_2$	$\alpha$
460	0.59	3.66e3	0.62	1.09	1.09

TABLE 4. Model parameters for the NMC battery.

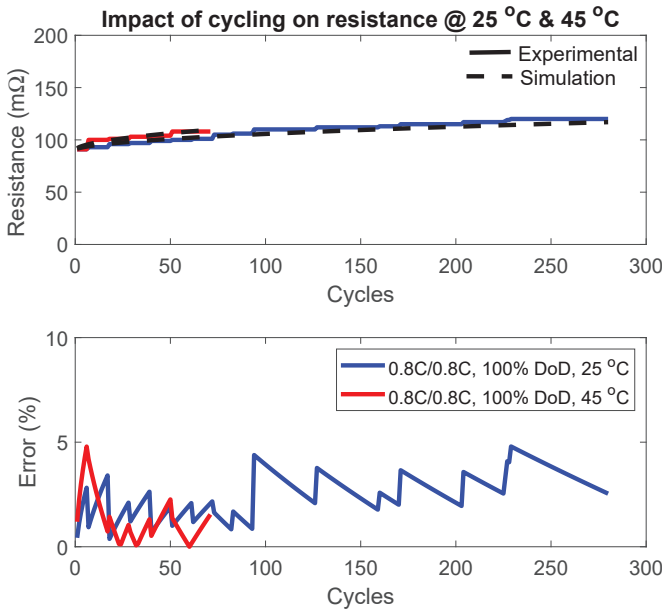


**FIGURE 18.** Impact of cycling at 25 °C and 45 °C ambient temperatures on battery resistance.

## V. CONCLUSION

This paper presented a cycle life model for lithium-ion batteries. The model is based on physical equations commonly used for fatigue analysis, and equivalent cycle counting, which makes it applicable to any lithium-ion battery types. The main contribution is a simplified parameter identification process using battery datasheets and limited (short duration) cycling tests. As most lithium-ion battery datasheets come with life cycle curves, the parameter identification process is less time consuming and less expensive. The model is able to represent the impact of common cycle life factors such as: depth-of-discharge (DoD), temperature and C-rate. The simulation results for two lithium-ion battery types (LFP-LiFePO<sub>4</sub> and NMC-LiNiMnCoO<sub>2</sub>) are close to reality with an absolute error of less than 1.5% on the battery capacity. The model also provided an absolute error of less than 5 % on the battery resistance. This makes the proposed model a good candidate for electrical simulation of lithium-ion battery cycling effects.

## REFERENCES

- [1] L. McCurlie, M. Preindl and A. Emadi "Fast Model Predictive Control for Redistributive Lithium-Ion Battery Balancing," *IEEE Trans. Ind. Electron.*, vol. 64, no. 2, pp. 1350-1357, Feb. 2017.
- [2] A. Uno and A. Kukita, "Cycle Life Evaluation Based on Accelerated Aging Testing for Lithium-Ion Capacitors as Alternative to Rechargeable Batteries," *IEEE Trans. Ind. Electron.*, vol. 63, no. 3, pp. 1607-1617, Mar. 2016.
- [3] Y. Xiao, "Model-Based Virtual Thermal Sensors for Lithium-ion Battery in EV Applications," *IEEE Trans. Ind. Electron.*, vol. 62, no. 5, pp. 3112-3122, May 2015.
- [4] A. Sidhu, A. Izadian and S. Anwar, "Adaptive Nonlinear Model-Based Fault Diagnosis of Li-ion Batteries," *IEEE Trans. Ind. Electron.*, vol. 62, no. 2, pp. 1002-1011, Feb. 2015.
- [5] J. Jiuchun, L. Qiujiang, Z. Caiping and Z. Weige, "Evaluation of Acceptable Charging Current of Power Li-Ion Batteries Based on Polarization Characteristics," *IEEE Trans. Ind. Electron.*, vol. 61, no. 12, pp. 6844-6851, Dec. 2014.
- [6] H. Chaoui, N. Golbon, I. Hmouz, R. Souissi and S. Tahar, "Lyapunov-Based Adaptive State of Charge and State of Health Estimation for Lithium-Ion Batteries," *IEEE Trans. Ind. Electron.*, vol. 62, no. 3, pp. 1610-1618, Mar. 2015.
- [7] R. Xiong, Y. Zhang, J. Wang, H. He, S. Peng and M. Pecht, "Lithium-Ion Battery Health Prognosis Based on a Real Battery Management System Used in Electric Vehicles," *IEEE Trans. Veh. Tech.*, vol. 68, no. 5, pp. 4110-4121, May 2019.
- [8] K. Li, F. Wei, K. J. Tseng and B. Soong, "A Practical Lithium-Ion Battery Model for State of Energy and Voltage Responses Prediction Incorporating Temperature and Ageing Effects," *IEEE Trans. Ind. Electron.*, vol. 65, no. 8, pp. 6696-6708, Aug. 2018.
- [9] G. W. You, S. Park and D. Oh, "Diagnosis of Electric Vehicle Batteries Using Recurrent Neural Networks," *IEEE Trans. Ind. Electron.*, vol. 64, no. 6, pp. 4885-4893, June 2017.
- [10] X. Hu, J. Jiang, D. Cao and B. Egardt, "Battery Health Prognosis for Electric Vehicles Using Sample Entropy and Sparse Bayesian Predictive Modeling," *IEEE Trans. Ind. Electron.*, vol. 63, no. 4, pp. 2645-2656, Apr. 2016.
- [11] A. El Mejdoubi, A. Oukaour, H. Chaoui, H. Gualous, J. Sabor and Y. Slamani, "State-of-Charge and State-of-Health Lithium-Ion Batteries Diagnosis According to Surface Temperature Variation," *IEEE Trans. Ind. Electron.*, vol. 63, no. 4, pp. 2391-2402, Apr. 2016.
- [12] X. S. Si, "An Adaptive Prognostic Approach via Nonlinear Degradation Modeling: Application to Battery Data," *IEEE Trans. Ind. Electron.*, vol. 62, no. 8, pp. 5082-5096, Aug. 2015.
- [13] R. Fu, S. -Y. Choe, V. Agubra and J. Fergus, "Development of a physics-based degradation model for lithium ion polymer batteries considering side reactions," *J. of Power Sources*, vol. 278, pp. 506-521, Mar. 2015.
- [14] S. J. Moura, J. C. Forman, S. Bashash, J. L. Stein and H. K. Fathy, "Optimal Control of Film Growth in Lithium-Ion Battery Packs via Relay Switches," *IEEE Trans. Ind. Electron.*, vol. 58, no. 8, pp. 3555-3566, Aug. 2011.
- [15] J. Wang, P. Liu, J. Hicks-Garner, E. Sherman, S. Soukiazian, M. Verbrugge, H. Tataria, J. Musser and P. Finamore, "Cycle-life model for graphite-LiFePO<sub>4</sub> cells," *J. of Power Sources*, vol. 196, pp. 3942-3948, Apr. 2011.
- [16] M. Petricca, D. Shin, A. Bocca, A. Macii, E. Macii and M. Poncino, "Automated generation of battery aging models from datasheets," in *32nd IEEE ICDD*, pp. 483-488, 2014.
- [17] F. Akar, Y. Tavlasoglu and B. Vural, "An Energy Management Strategy for a Concept Battery/Ultracapacitor Electric Vehicle With Improved Battery Life," *IEEE Trans. Transport. Electrification*, vol. 3, no. 1, pp. 191-200, Mar. 2017.
- [18] J. Shen, S. Dusmez and A. Khaligh, "Optimization of Sizing and Battery Cycle Life in Battery/Ultracapacitor Hybrid Energy Storage Systems for Electric Vehicle Applications," *IEEE Ind. Informatics*, vol. 10, no. 4, pp. 2112-2121, Nov. 2014.
- [19] X. Han, M. Ouyang, L. Lu and J. Li, "A comparative study of commercial lithium ion battery cycle life in electric vehicle: Capacity loss estimation," *J. of Power Sources*, vol. 268, pp. 658-669, Dec. 2014.
- [20] C. -Y. Chang, P. Tulpule, G. Rizzoni, W. Zhang and X. Du, "A probabilistic approach for prognosis of battery pack aging," *J. of Power Sources*, vol. 347, pp. 57-68, Apr. 2017.
- [21] A. Cordoba-Arenas, S. Onori, Y. Guezenne and G. Rizzoni, "Capacity and power fade cycle-life model for plug-in hybrid electric vehicle lithium-ion battery cells containing blended spinel and layered-oxide positive electrodes," *J. of Power Sources*, vol. 278, pp. 473-483, Mar. 2015.
- [22] N. Omar, M. A. Monem, Y. Firouz, J. Salminen, J. Smekens, O. Hegazy, H. Gualous, G. Mulder, P. Van den Bossche, T. Coosemans and J. Van Mierlo, "Lithium iron phosphate based battery Assessment of the aging parameters and development of cycle life model," *Applied Energy*, vol. 113, pp. 1575-1585, Jan. 2014.
- [23] T. Messahi, N. Rizoug, P. Bartholome, R. Sadoun, F. Khenfri, and P. Le Moigne, "Dynamic Model of Li-Ion Batteries Incorporating Electrothermal and Ageing Aspects for Electric Vehicle Applications," *IEEE Ind. Electron.*, vol. 65, no. 2, pp. 1298-1305, Feb. 2018.
- [24] M. Ecker, J. B. Gerschler, J. Vogel, S. Kabitz, F. Hust, P. Dechant and D. U. Sauer, "Development of a lifetime prediction model for lithium-ion batteries based on extended accelerated aging test data," *J. of Power Sources*, vol. 215, pp. 248-257, May 2012.



- [25] J. M. Reniers, G. Mulder and D. A. Howey, "Review and Performance Comparison of Mechanical-Chemical Degradation Models for Lithium-Ion Batteries," *J. Electrochem. Soc.*, vol. 166, pp. A3189-A3200, Sept. 2019.
- [26] X. Jin, A. Vora, V. Hoshing, T. Saha, G. Shaver, O. Wasynczuk and S. Varigondar, "Applicability of available Li-ion battery degradation models for system and control algorithm design," *Control Eng. Practice*, vol. 71, pp. 1-9, Nov. 2017.
- [27] B. Xu, A. Oudalov, A. Ulbig, G. Andersson and D. Kirschen, "Modeling of Lithium-Ion Battery Degradation for Cell Life Assessment," *IEEE Trans. Smart Grid*, vol. 9, no. 2, pp. 1131-1140, March 2018.
- [28] H. Beltran, J. Barahona, R. Vidal, J. C. Alfonso, C. Arino and E. Perez, "Ageing of different types of batteries when enabling a PV power plant to enter electricity markets," in *42nd IECON IEEE Ind. Electron. Society*, pp. 1986-1991, 2016.
- [29] S. N. Motapon, A. Lupien-Bedard, L.-A. Dessaint, H. Fortin-Blanchette and K. Al-Haddad, "A Generic Electrothermal Li-ion Battery Model for Rapid Evaluation of Cell Temperature Temporal Evolution," *IEEE Ind. Electron.*, vol. 64, no. 2, pp. 998-1008, Feb. 2017.
- [30] M. W. Verbrugge and Y.-T. Cheng, "Stress and Strain-Energy Distributions within Diffusion-Controlled Insertion-Electrode Particles Subjected to Periodic Potential Excitations," *J. Electrochem. Soc.*, vol. 156, pp. A927, Oct. 2009.
- [31] C. Dudezert, Y. Reynier, J.-M. Duffault, S. Franger, "Fatigue damage approach applied to Li-ion batteries ageing characterization," *Materials Sc. Eng.*, vol. 213, pp. 177-189, Nov. 2016.
- [32] K. Smith, M. Earleywine, E. Wood, J. Neubauer, and A. Pesaran, "Comparison of Plug-In Hybrid Electric Vehicle Battery Life Across Geographies and Drive Cycles," *SAE Int.*, Apr. 2012.
- [33] I. Laresgoiti, S. Kabit, M. Ecker, D. U. Sauer, "Modeling mechanical degradation in lithium ion batteries during cycling: Solid electrolyte interphase fracture," *J. of Power Sources*, vol. 300, pp. 112-122, Dec. 2015.
- [34] H. Xuebing, L. Languang, Z. Yuejiu, F. Xuning, L. Zhe, L. Jianqiu and O. Minggao, "Review on the key issues of the lithium ion battery degradation among the whole life cycle," *eTransportation*, vol. 1, Aug. 2019.



**SOULEMAN N. MOTAPON** (M'09) received the M.Sc. degree in power electronics and drives from Aalborg University, Aalborg, Denmark, in 2005, and the M.Eng and Ph.D. degrees in electrical engineering from the Ecole de Technologie Supérieure (ETS), Université du Québec in Montreal, in 2008 and 2013, respectively.

From 2010 to 2012, he was with Clipper Windpower/Pratt & Whitney power systems, as a Senior Electrical Engineer. From 2013 to 2019, he was leading the Power Electronics group at XZERES Wind, Wilsonville, OR, USA. Since 2020, he is a Senior Power Conversion Design Engineer at Vanner, Hilliard, OH, USA. His research interests include high efficiency, ultrahigh power density DC-DC and DC/AC converters for vehicles, wind turbine, solar and battery systems. He is also a Researcher with the Ecole de Technologie Supérieure, working on modeling and testing of new technologies Li-ion batteries and hybrid capacitors.



transfer applications.

**ENRIC LACHANCE** received the B.Sc. and M.Sc. degrees in electrical engineering from the Ecole de Technologie Supérieure (ETS), Université du Québec in Montreal, in 2015 and 2018, respectively.

He spent a number of years in the petroleum and nuclear industry. He is currently teaching electrical engineering at Montmorency College, Laval, QC. His current research interest is the geometric influence in the magnetic core design for power



**LOUIS-A. DESSAINT** (M'88-SM'91-F'13) received the B.Eng., M.Sc.A., and Ph.D. degrees from the Ecole Polytechnique de Montreal, Montreal, P.Q., Canada, in 1978, 1980 and 1985, respectively, all in electrical engineering. He is currently Professor at the Ecole de Technologie Supérieure, Université du Québec in Montreal. He is an author of the MathWorks "SimPowerSystems" (SPS) Blockset.

Professor Dessaint was the holder of the Hydro-Quebec TransEnergie Chair on the simulation and control of power systems from 2001 to 2011 and the ETS institutional Chair on the safety of power systems from 2013 to 2016. He was associate editor of the IEEE Transactions on Control Systems Technology from 2009 to 2013 and of IET Generation, Transmission & Distribution until 2015.

Dr. Dessaint is a Fellow of the Canadian Academy of Engineering and a member of the Cercle d'excellence de l'Université du Québec.



**KAMAL AL-HADDAD** (S'82-M'88-SM'92-F'07, LF'20) received the B.Sc.A. and M.Sc.A. degrees from the University of Quebec a Trois-Rivieres, Trois-Rivieres, QC, Canada, in 1982 and 1984, respectively, and the Ph.D. degree from the Institut National Polytechnique, Toulouse, France, in 1988.

Since June 1990, he has been a Professor with the Electrical Engineering Department, Ecole de Technologie Supérieure (ETS), Montreal, QC, where he has been the holder of the senior Canada Research Chair in Electric Energy Conversion and Power Electronics since 2002. He has supervised more than 170 Ph.D. and M.Sc.A. students in the field of power electronics. He is a Consultant and has established very solid link with many Canadian industries working in the field of power electronics, energy conversion, electric transportation, renewable energy, multilevel topologies, aeronautics, and telecommunications. He has coauthored more than 600 transactions and conference papers as well as two books.

Prof. Al-Haddad is a fellow member of the Canadian Academy of Engineering. He is IEEE IES President 2016-2017, Associate editor of the Transactions on Industrial Informatics, IES Distinguished Lecturer and recipient of the 2014 IEEE IES Dr.-Ing. Eugene Mittelmann Achievement Award. Prof. Al-Haddad is a member of the Academy of Sciences and fellow of the Royal Society of Canada.